Case Studies in Construction Materials 20 (2024) e02793

Contents lists available at ScienceDirect

Case Studies in Construction Materials

journal homepage: www.elsevier.com/locate/cscm

The effect of the geometrical properties of geocell reinforcements between a two-layered road structure under overload conditions

Burak Evirgen [a,*], Halil Oğuzhan Kara [b], Muhammed Sefa Ucun [a], Asker Alp Gültekin [a], Mert Tos [a], Volkan Öztürk [a]

[a] Department of Civil Engineering, Eskisehir Technical University, 26555, Eskişehir, Türkiye
[b] Department of Civil Engineering, Kastamonu University, 37150, Kastamonu, Türkiye

ARTICLE INFO

Keywords:
Geocell
Flexible pavement
Large-scale test
Plate load test
Finite element modeling

ABSTRACT

Depending on the project traffic, the total thickness of a granular base can reach excessive values. Granular layers of large thicknesses undoubtedly extend the duration of a project and cause high project total costs. In this study, the improvement in settlement behaviour of unbound granular base layers reinforced with geocell was investigated by way of large-scale laboratory tests and finite element modeling. Plate loading tests were performed on unreinforced and geocell reinforced base layers, which were constructed on subgrade soil with a low bearing capacity under 1750 kPa overload condition. It was determined that the amount of settlement observed at the same stress levels decreased with an increase in the aperture size from 440 mm to 660 mm and the geocell height from 100 mm to 150 mm. The reduction in settlement potential, which reached 78% compared to the unreinforced reference section around 25 kPa, decreased to 55% at around a 200 kPa standard load. With an increase in the vertical stress level, the effectiveness of geocell reinforcement decreases and a serious decrease occurs after 500 kPa, becoming completely unserviceable when a level of 1000 kPa is to be exceeded. Although the difference between the experimental results and the modeling values remained below 5% in the reference section, it reached as high as 30% differences in the geocell implemented sections up to 200 kPa, due to three-dimensional geocell adaptation problems within the finite element calculations. In this way, it will be possible to increase the performance of road surfaces by keeping the pavement thickness constant, and also it will be possible to design more economical sections by reducing the required thickness.

1. Introduction

The need for effective methods to extend the service life of road structures remains because of the maintenance, repair and operating costs of existing roads, and is gaining importance. One of these methods is the use of a geosynthetic material between base layers since it has specific advantages, such as ease of applicability, long term performance, a low maintenance requirement, and high tensile strength. On the other hand, a relatively new three-dimensional geosynthetics provides extra confinement effects owing to its three-dimensional working principle around soil cells. Geocell is a soil reinforcement and erosion protection material with a honeycomb texture made of a high-density polyethylene alloy. Moreover, it affects the cost of the road and environment positively since the average construction cost can be reduced about 10% and CO_2 emission can be decreased by using geocell [1].

* Corresponding author.
E-mail address: burakevirgen@eskisehir.edu.tr (B. Evirgen).

https://doi.org/10.1016/j.cscm.2023.e02793
Received 11 August 2023; Received in revised form 22 November 2023; Accepted 13 December 2023
Available online 17 December 2023

There have been experimental studies on the use of geosynthetic materials as a base reinforcement in the field of transportation [2–4], or as subbase reinforcement [5,6]. Also, geocell performance has been examined with different soil types. When it is used with sand beds, the bearing capacity increased by four times, and by almost three times in the clay beds [7]. In addition, a number of studies focus on the loading mechanism in terms of static or cyclic procedure [8–15]. The location of geosynthetic material is another challenge depending on the tensile strength, subgrade modulus, type of footing, and soil-geosynthetic interaction [16–18]. The most effective position of the reinforcement in the single-reinforced case is proposed as one fourth the height of the layer of the distance from the ground surface [19]. The soil reinforced with cellular fill showed up to 524% higher bearing capacity [20], a decrease up to 56.1% soil pressure [9], as well as providing a reduction in total settlement by 40% [21] compared to an unreinforced case. However, excessive settlements occur after geocell material loses its function if the ratio between the embedded depth and width of the foundation rises above 0.9 [22]. The length and the number of the reinforcement layers have a positive effect on soil improvement level [18]. Furthermore, geocell material produced in a friction-increasing structure gives better performance compared to smooth surface geocell material [23]. It was concluded that the reinforcement method using geocell is more effective than other types of geosynthetics, due not only to transferring the foundation load into deeper points, but by also reducing the observed stress and deformation characteristics as well as improving the effectiveness of vibration mitigation [7,24–26]. Also, geocell shows the best performance with sand according to the reinforcement effect under the high level of bearing pressure when it is compared to other geosynthetic [27].

The finite element method, which is a widely accepted numerical approach worldwide, is also used by researchers to evaluate the results of geosynthetic reinforced works [28–33]. These numerical studies in the literature show that the bearing capacity and stiffness of soils reinforced with geosynthetic material increase significantly, in addition to a decrease in settlement. Similarly, the settlement reduction impact on the geocell mat system is studied to decrease the harmful effects of deformation and stress on the buried flexible pipes under the road structure by using a finite element program [34]. The best stiffness behaviour was taken for the geocell reinforcement for the data to be 1000 kPa within the investigation about the pressure-settlement behavior of reinforced sand with geocell overlying soft clay by using Abaqus [35]. In addition, experimental studies were validated with numerical models by way of Flac3D and Abaqus, commonly [7,35,36].

Although there are many studies regarding the utility of geosynthetic materials in road layers in the literature, most of these investigated the behavior of geosynthetic materials of around a 200 kPa road load, which is accepted as a standard load within general usage. In particular, these studies were generally carried out within wide range of load levels for geocell reinforcements from 160 kPa to 1000 kPa [14,27,34,37–40], while 1000 kPa value was reached in limited studies [41]. Within the scope of this study, the behavior and strength parameters of four different geocells with high axial stiffness under overload conditions of up to 1750 kPa were examined from both an experimental and a modeling point of view to decrease the thickness of pavement unbound granular base layers as well as to determine the effect of the size of the geocell. It is new in terms of the behavior of the geocell material under excessive load and the determination of the load level at which the structure of the geocell material deteriorates and loses its function completely, under unexpected loading conditions due to repeated loading of overloaded trucks or natural disasters such as debris flow or avalanche.

2. Material properties

2.1. Soil

In general, strong base layers were constructed above the problematic natural subgrade, having a low bearing capacity or an excessive settlement potential, in site applications whether a stabilized road or an asphaltic pavement. Therefore, a subgrade soil was prepared with 25% of kaolinite clay and 75% of silica sand to satisfy the low California Bearing Ratio (CBR) level of less than 8% [3,4,11,12,16–18], as well as actual plant mix base material, which is frequently used as a granular fill in highway construction, being taken from a stone pit (Fig. 1). While a soil type of the clay-sand mixture material was determined silty sand (SM), the plant mix was determined as well graded gravel (GW) according to Unified Soil Classification System [42]. The geotechnical properties of the aforementioned soils are given in Table 1.

2.2. Geotextile

A single layered geotextile was used to serve as a separation between the subgrade, representing the natural soil layer with low bearing capacity, and the base on behalf of the stabilized layer both inside the reference test without geocell and the geocell-reinforced sections (Fig. 2) [47–51]. The properties of the geotextile material used for this purpose are given in Table 2 according to the manufacturer's values.

2.3. Geocell

In the reinforced experimental sections, four different types of geocell material were placed onto a geotextile of varying aperture and height to obtain the geometrical effects and related confinement. Within this purpose, the aperture and the height dimensions parameters were chosen as 358/258 mm-485/353 mm, and 100 mm-150 mm in open state of geocells (Fig. 2c). While the nominal thickness of the geocells used was 1.4 mm a constant parameter, the specimens were classified due to their closed dimensions of 440 mm and 660 mm (Table 3). So, 440 × 100 abbreviation denotes the aperture and the height dimensions of geocells in closed state, respectively.

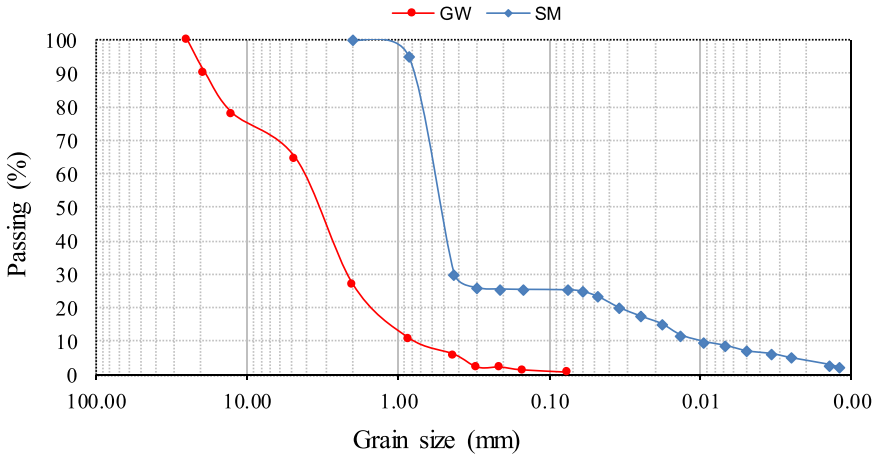

Fig. 1. Granulometry curve.

Table 1
Geotechnical properties of the soils used.

Property	Unit	GW	SM	Related Standard
Liquid limit	%	15.35	46.09	[43]
Plastic limit	%	13.91	44.70	
Plasticity index (PI)	%	1.44	1.39	
Shrinkage limit	%	-	6.46	
Maximum dry unit weight	kN/m^3	22.86	20.70	[44]
Optimum water content	%	7.10	11.67	
CBR	%	32.23	7.86	
Friction angle	°	54.3	35.4	[45]
Cohesion	kN/m^2	26.2	41.4	
Specific gravity	-	2.75	2.61	[46]

3. Experimental method

It should be noted that, the selection of an adequate box size is an essential point to represent actual soil behavior in terms of settlement and pressure distribution. A large-scale cubic soil box was designed with a 1500 mm unit dimension in order to eliminate boundary effects, considering the previous work having variable unit dimensions of between 500 mm and 2000 mm according to the type of soil, the size of the loading plate and the applied pressure [3,4,11,12,16–18]. A 300 mm diameter was chosen for the rigid steel loading plate, since the optimum improvement was achieved using an experimental setup with a width of between four to eight times the diameter of the loading plate [58–60]. A fully enclosed box was obtained, after the bottom and side faces, but not the front side, were covered with 8 mm thick steel sheets on a steel frame. Removable steel angle profiles, which have a 100 mm equal width, were assembled in front of the cell in order to measure the prescribed compaction levels layer by layer and to enclose the cell.

First of all, the subgrade soil representing the natural condition was laid in four layers with a total thickness of 90 cm from the bottom of the box with the help of a mobile conveyor, after mixing with an optimum amount of water content inside a concrete mixer (Fig. 3(a)). The granular base representing the stabilized fill was laid on the subgrade with a total thickness of 40 cm. Each layer was compacted up to the desired level by way of a compactor with two passes along both directions according to proctor tests (Fig. 3(b)). In this way, a regular honeycomb structure of cells was provided. In all the test sections, including the reference case without geocell, geotextile was placed between two soil interfaces at a height of 90 cm from the bottom, while the additional geocell elements were positioned on the geotextile in the case of reinforced sections (Fig. 3(c)). On the other hand, sand cone experiments were realized to verify the anticipated relative densities [61]. According to the average results obtained from the experiments performed in all the sections, relative compaction values were found to be 98.76% and 90.11% for a stabilized fill base (GW) and natural subgrade (SM) layers, respectively.

While the pressure was applied with a 300 kN capacity hydraulic jack at the center location on the soil surface, the settlement values were measured by two linearly variable 50 mm capacity displacement transducers (lvdt) on the loading plate at a central location, simultaneously (Fig. (3d)). In addition, 250 mm capacity three coupled lvdts were located at the 30 cm, 45 cm and 60 cm distances along horizontal axis with respect to the center point within the purpose of collecting the surface settlement distribution. Soil pressure gauges with a capacity of 500 kPa were placed at 80 cm and 60 cm depths from the ground surface, which are equal to 20 cm and 40 cm below the interface of soils, respectively (Fig. (3d)).

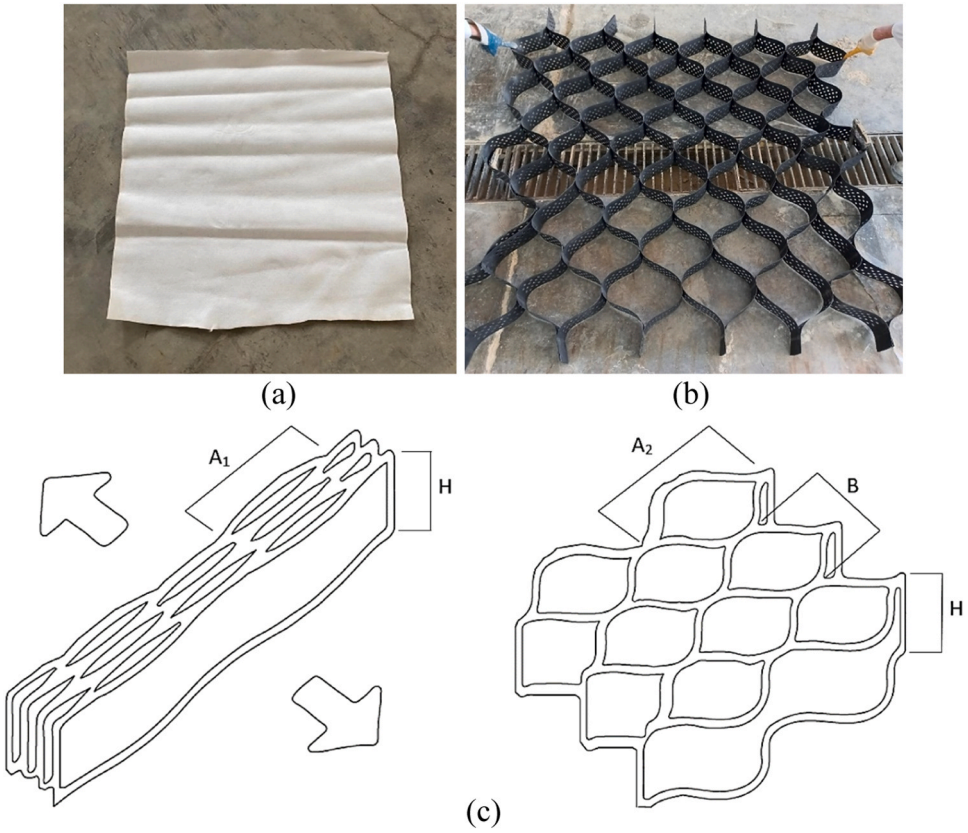

Fig. 2. Sample of geosynthetic materials used; (a) Geotextile, and (b-c) Geocell.

Table 2
Properties of the geotextiles used.

Property	Unit	Value
Weight per unit area	g/m^2	500 (−0/+40)
Tensile strength	kN/m	31 (−4)
Elongation at break	%	≥ 50
Static puncture resistance	N	5800 (−500)
Opening size	mm	0.075 (± 0.025)
Water permeability	$l/(sm^2)$	42 (± 15)
Roll width	M	2-6 (± 0.1)
Roll length	m	50 (± 1)

Table 3
Properties of the geocells used according to manufacturer values.

Property	Unit	Type of Geocell		Related Standard
		440 × 100 440 × 150	660 × 100 660 × 150	
Nominal sheet thickness after texturing	mm	1.4(± 0.1)	1.4(± 0.1)	[52,53]
Tensile strength of strips (Without perforation)	kN/m	≥ 21	≥ 21	[54]
Tensile strength of strips (With perforation)	kN/m	≥ 12,6	≥ 12,6	
Weld shear strength	kN/m	≥ 21	≥ 22	[55]
Weld peel strength	kN/m	≥ 10	≥ 9	
Carbon black content	%	≥ 1.5	≥ 1.5	[56]
Polymer density	g/cm^3	≥ 0.935	≥ 0.935	[57]
Aperture width (A_1)	mm	440	660	-
Aperture width (A_2/B)	mm	358B258	485/353	-
Strip height	mm	100-150	100-150	-
Cell area	mm	≥ 455	≥ 855	-

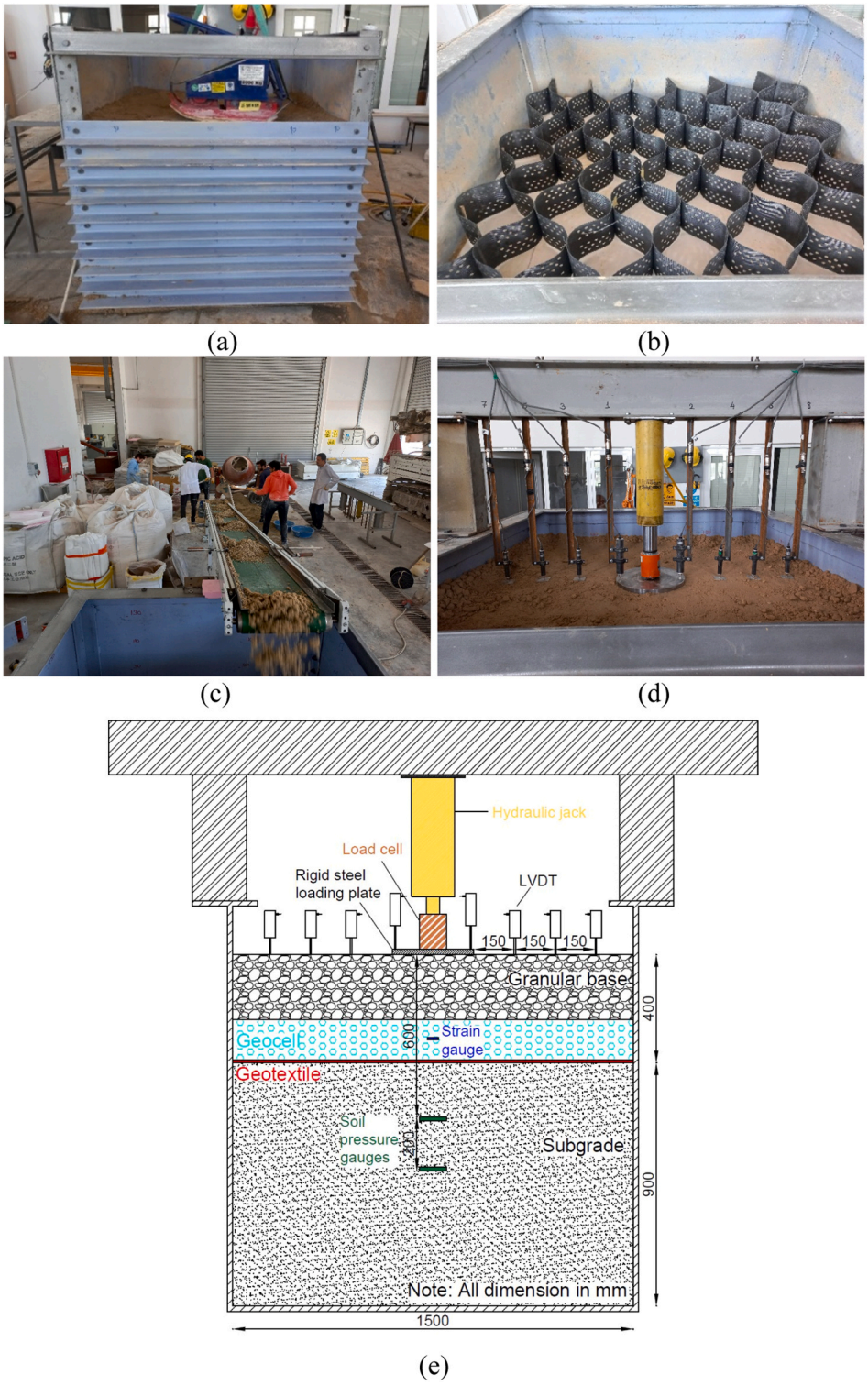

Fig. 3. (a) Experimental soil box, (b) Adopted geosynthetics between road layers, (c) Preparation and transportation of soil inside box, (d) Experimental setup, and (e) Details of instrumentation.

4. Finite element modeling

The finite element models were defined in Plaxis 3D for five different sections, the same as the experimental studies, considering the ability of this software to model a wide variety of geotechnical problems and its user-friendly interface. Plaxis has a finite element solution scheme to solve initial and boundary problems, using a required amount of iteration in order to minimize errors by reaching the correct value with the help of nodes. Plaxis 3D was selected in modeling procedure instead of other finite element software, since it is the most preferred software in the field of geotechnical engineering field worldwide.

First of all, the soil volume was drawn with dimensions of 1.5 m x 1.5 m x 1.3 m according to the experimental soil box. The linear elastic-perfect plastic Mohr-Coulomb model, which is suitable for subbase application and can analyze faster than other material models, was used to simulate the silty sand type (SM) of natural subgrade layer and well graded gravel type of (GW) stabilized base layer [23,62]. The sections were studied under undrained conditions as they contain clay content in a closed experimental cell. The unit weight and shear strength parameters obtained from the laboratory tests were directly used, while two third of the experimental results of the modulus of elasticity values of soils were chosen after consideration a reduction factor was applied for undrained deformation modulus according to the unconfined compression test results, because the lack of undrained triaxial test data [63,64]. In addition, the values related with Poisson's ratio [65,66], interface strength [67,68] and permeability [69–71] were calculated based on the literature correlations as given in Table 4.

The solid state three-dimensional complex honeycomb structure of the geocells was imported into the model, after sketching in a tetragonal shape with the help of Autocad, due to the real sizes as given in Table 3 and Fig. 4(a) [62]. This geocell material is defined as

Table 4
Mohr-Coulomb model soil parameters.

	Symbol	Unit	GW	SM
Material model	Model	-	Mohr-Coulomb	Mohr-Coulomb
Drainage type	Type	-	Undrained	Undrained
Dry unit weight	γ_{unsat}	kN/m^3	22.86	20.70
Saturated unit weight	γ_{sat}	kN/m^3	23.94	22.95
Vertical permeability coefficient	k_y	m/day	0.01	0.0001
Horizontal permeability coefficient	k_x	m/day	0.01	0.0001
Modulus of elasticity	E	kN/m^2	10650	3650
Poisson's ratio	ν	-	0.30	0.30
Cohesion	c	kN/m^3	26.20	41.4
Internal friction angle	Φ	°	54.30	35.4
Dilatancy angle	Ψ	°	24.30	5.40
Geogrid-ground interface coefficient	R_{inter}	-	0.70	0.70

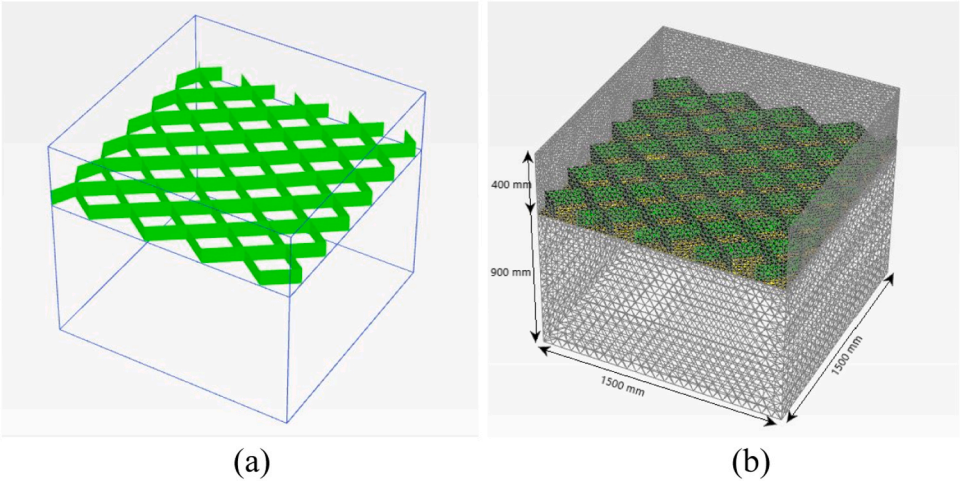

Fig. 4. (a) The location and details of a 440 × 100 type of geocell and (b) Transparent appearance with mesh contours.

Table 5
Properties of geotextile and geocell.

	Symbol	Unit	Geotextile	Geocell	Material Type
Axial Stiffness	EA	kN/m	60	504	Elastic

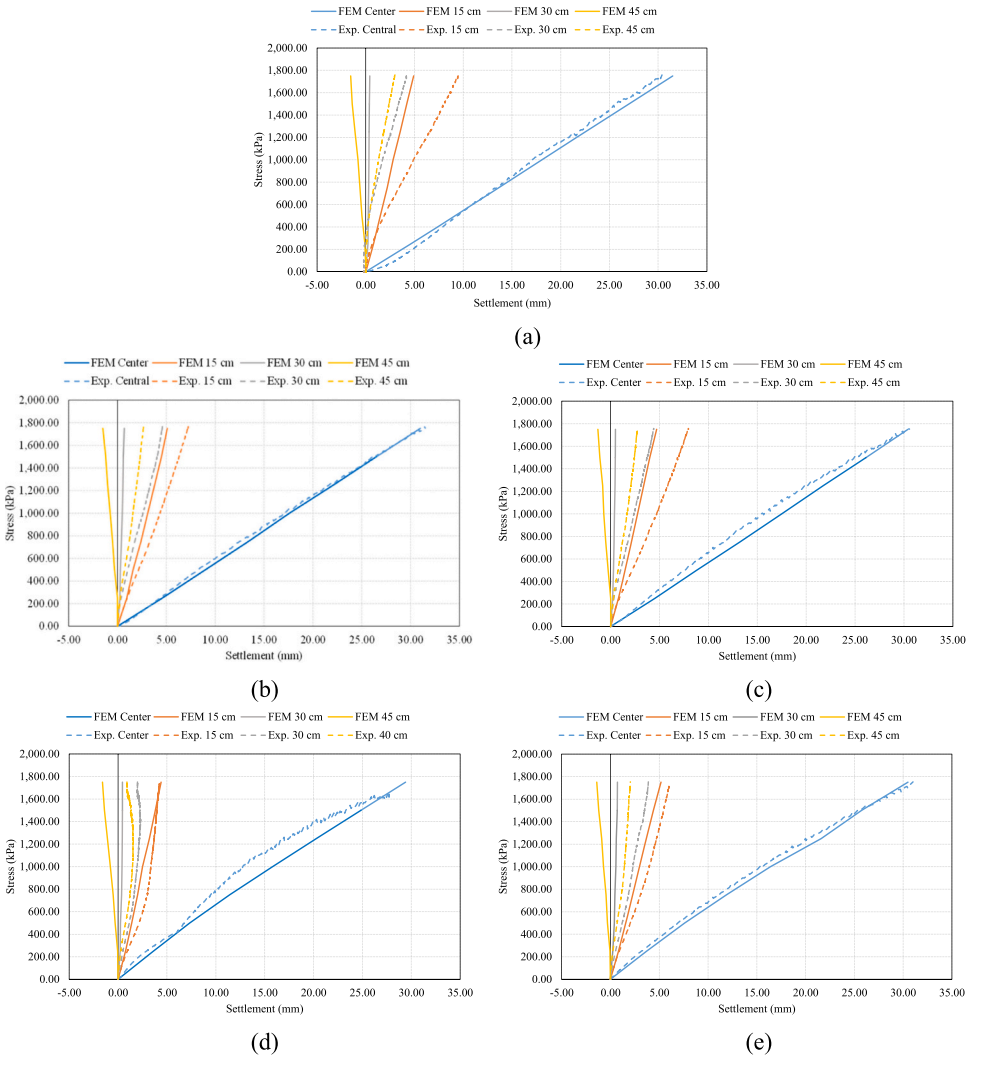

Fig. 5. The vertical stress vs. settlement graphs; (a) Reference section, (b)-(e) Reinforced sections by 440 × 100, 440×150, 660×100 and 660×150 types of geocell, respectively.

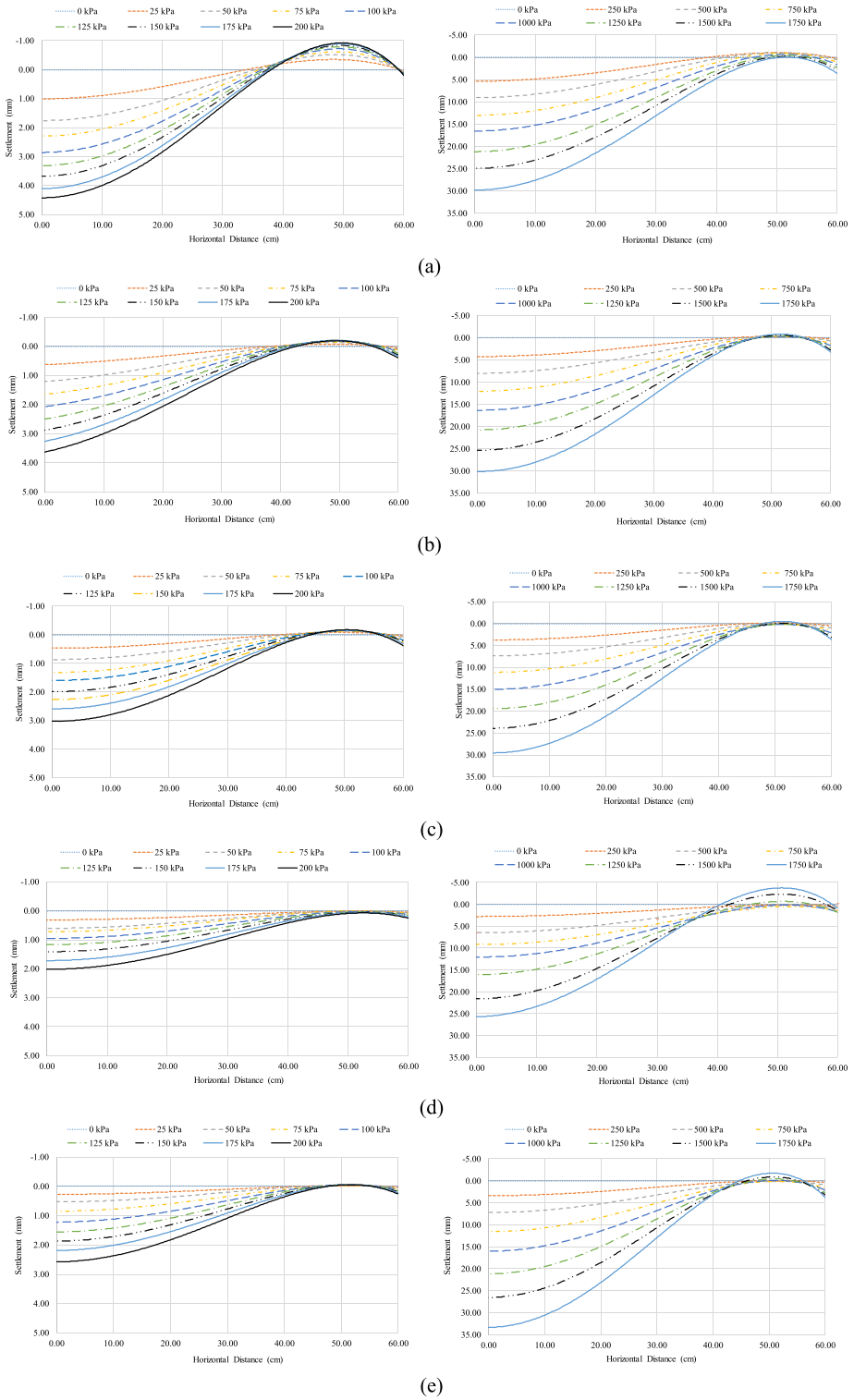

Fig. 6. The change in surface settlements due to applied load level and horizontal distance; (a) Reference section, (b)-(e) Reinforced sections by 440 × 100, 440×150, 660×100 and 660×150 types of geocell, respectively (up to 200 kPa - left and 1750 kPa - right).

a linear-elastic geosynthetic type structural element. While geogrid materials can resist tensile stresses, they do not have enough resistance against bending in a planar form. Therefore, the axial stiffness values of the used geosynthetics were calculated according to the tensile strength of perforated strip tested in line with the data obtained from the manufacturer. The axial stiffness of the geocell was calculated with respect to the tensile strength corresponding to 2.5% elongation according to the manufacturer parameters (Table 5), although geotextile elongation at break was determined from the tensile strength at a minimum 50% elongation [54]. As in the use of geocells with high axial stiffness, which is another aim of this study, this parameter can be found in the literature from 340 kN/m to 465 kN/m for high density polyethylene geocells [23,72,73].

Vertical pressure was applied on a 300 mm rigid steel plate in the center position, the same as the experimental process up to the 1750 kPa. The boundary conditions of model were constrained along horizontal directions, although the displacements through the vertical direction of all the edge surfaces were allowed. At the base of the model, constraints were applied along all the directions similar with experimental box. The groundwater level was defined at the lower base, since the optimum water content values the soils were defined with the unit weights and experimental soil box which was not at a saturated state. Mesh elements were selected as 10-node, while there were 151238 and 74616 elements inside the 900 mm thick layer of subgrade and a 400 mm thick layer of granular base above it, respectively. Along the ground surface zone, where the deformation and stress concentration are intense, denser elements and fine mesh were used, even though a medium mesh was used in the remaining parts of soil (Fig. 4(b)). During the staged construction type of the scenario the following operations were kept in step, the subgrade layer was defined, and the stabilized granular base was activated after placing of the geotextile and geocell, and a 1750 kPa surface load was applied to the soil surface. The significant point to be considered in these stages is activation of the 'update mesh' option from the deformation control parameters during the geotextile and geocell placement phase.

5. Results and discussion

5.1. Experimental results

The applied vertical stress at the center location versus settlement graphs due to the plate loading tests are given in Fig. 5, which were performed on the four different geocell reinforced sections in addition to reference one without geocell. The aim was to determine the overload conditions by reaching a vertical stress level of 1750 kPa. For the reference section under peak stress level, the settlement values obtained on the soil surface at the center axis and 15 cm, 30 cm and 45 cm distances from the edge of steel loading plate are 30.74 mm, 9.57 mm, 4.26 mm and 3.03 mm, respectively. Although similar settlement results were obtained in the center axis, particularly under high vertical stress, serious differences occurred from the center axis to the outer walls of the test box as a result of the spreading load by geocell.

In order to analyze the more detailed trends, settlement curves were plotted with respect to a horizontal distance representing the spacing between the center axis and the surface measurement points under gradual stress increments. These loading levels were given as 25kPa and 250kPa for a standard load and heavy load conditions, while surface settlements indicate the averages of oppositely positioned displacement gauges (Fig. 6). The highest settlement values were naturally observed at the center location, where the load is applied onto the lading plate, and it was determined that the general collapse behavior at that point appeared as heaving at progressive load levels. This characteristic is particularly prominent in the 660×100 type of geocell reinforced section, especially. At low load levels, the vertical stress concentration was propagated by the geocells according to the increase of confinement effect even if enhancement ratios differentiated for geocell types. It is thought that the applied pressure is not spread correctly by the geocell at high load levels, especially in 660×100mm geocell including section, due to the larger aperture geometry or insufficient height to create an amount of required confinement. There is a possibility that the cell may have settled together with the soil inside.

Tables 6 and 7 show the comparison between observed ground settlements and related decrease with respect to the reference case for standard and overload conditions. When compared with the reference test at a low stress level of around 25kPa, the settlement decrement changes between 37.09% and 78.14%, although the change in settlement reaches from a 9.84% decrease to a 3.62% increase at an overload condition in the case of geocell reinforced sections. The larger aperture size and cell height created more effective results in terms of general tendency.

The change in soil pressures through vertical direction are given in Fig. 7. In the case of applying a vertical stress of 1750 kPa from the surface, a stress reduction was observed around 83% and 87% for the reference section at a depth of 60 cm and 80 cm, respectively. In

Table 6
The change in settlement values under standard load up to 200 kPa.

Stress (kPa)	Settlement (mm) Reference	Settlement (mm) 440×100 geocell	Decrease (%)	Settlement (mm) 440×150 geocell	Decrease (%)	Settlement (mm) 660×100 geocell	Decrease (%)	Settlement (mm) 660×150 geocell	Decrease (%)
25	1.21	0.77	36.70	0.50	58.97	0.33	72.58	0.27	78.14
50	1.91	1.20	37.09	0.92	51.90	0.59	68.94	0.51	73.26
75	2.48	1.63	34.44	1.39	44.01	0.77	69.18	0.82	67.17
100	3.08	2.05	33.66	1.68	45.58	0.98	68.29	1.17	62.12
125	3.57	2.46	30.93	2.08	41.65	1.23	65.43	1.49	58.35
150	3.98	2.82	29.12	2.37	40.50	1.49	62.58	1.79	55.09
175	4.41	3.22	27.06	2.70	38.74	1.81	58.99	2.09	52.58
200	4.74	3.51	26.09	3.16	33.47	2.12	55.25	2.46	48.18

Table 7
The change in settlement values under overload up to 1750 kPa.

Stress (kPa)	Settlement (mm) Reference	Settlement (mm) 440 × 100 geocell	Decrease (%)	Settlement (mm) 440 × 150 geocell	Decrease (%)	Settlement (mm) 660 × 100 geocell	Decrease (%)	Settlement (mm) 660 × 150 geocell	Decrease (%)
250	5.62	4.38	22.11	3.86	31.35	2.91	48.34	3.22	42.74
500	9.41	8.30	11.72	7.59	19.32	6.80	27.72	6.98	25.78
750	13.46	12.53	6.97	11.51	14.51	9.62	28.58	11.01	18.20
1000	17.06	17.03	0.16	15.72	7.88	12.76	25.21	15.57	8.73
1250	21.83	21.67	0.73	20.12	7.83	17.24	21.04	20.18	7.58
1500	25.72	26.50	-3.04	24.85	3.39	23.30	9.42	25.60	0.45
1750	30.74	31.51	-2.49	30.55	0.63	27.72	9.84	31.86	-3.62

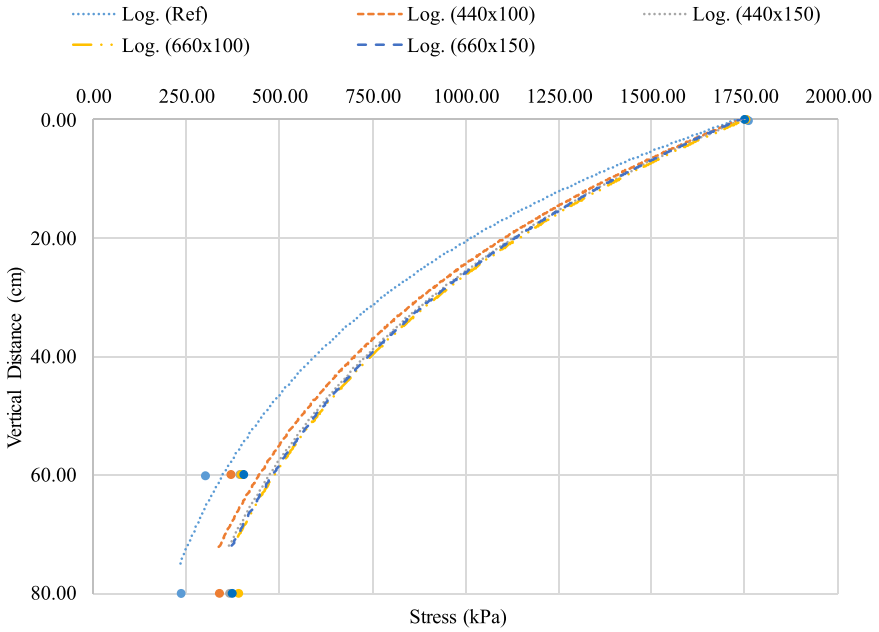

Fig. 7. The change in simultaneous soil pressures along the vertical direction.

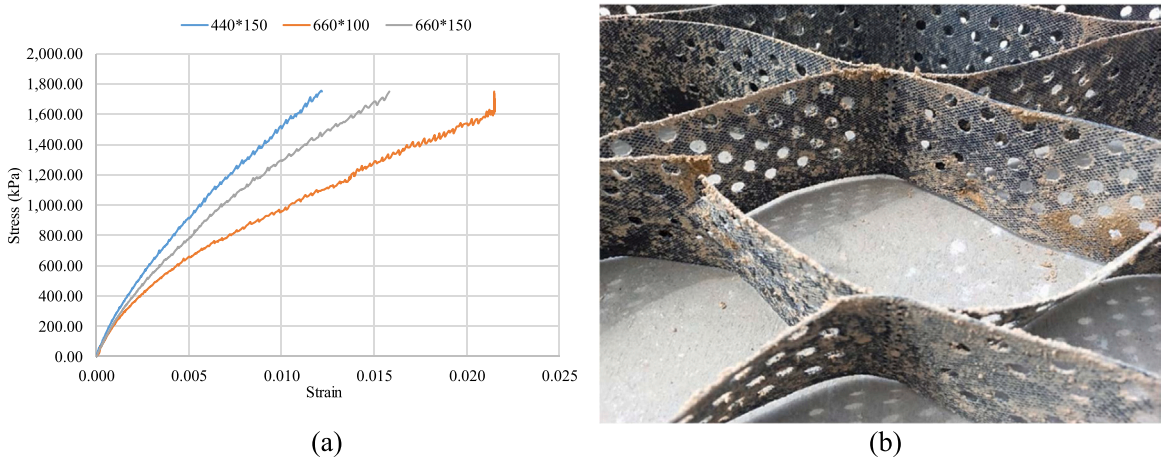

Fig. 8. (a) Stress - strain values of geocells due to strain gauges, (b) A failure caused from tearing and excessive spreading of cell.

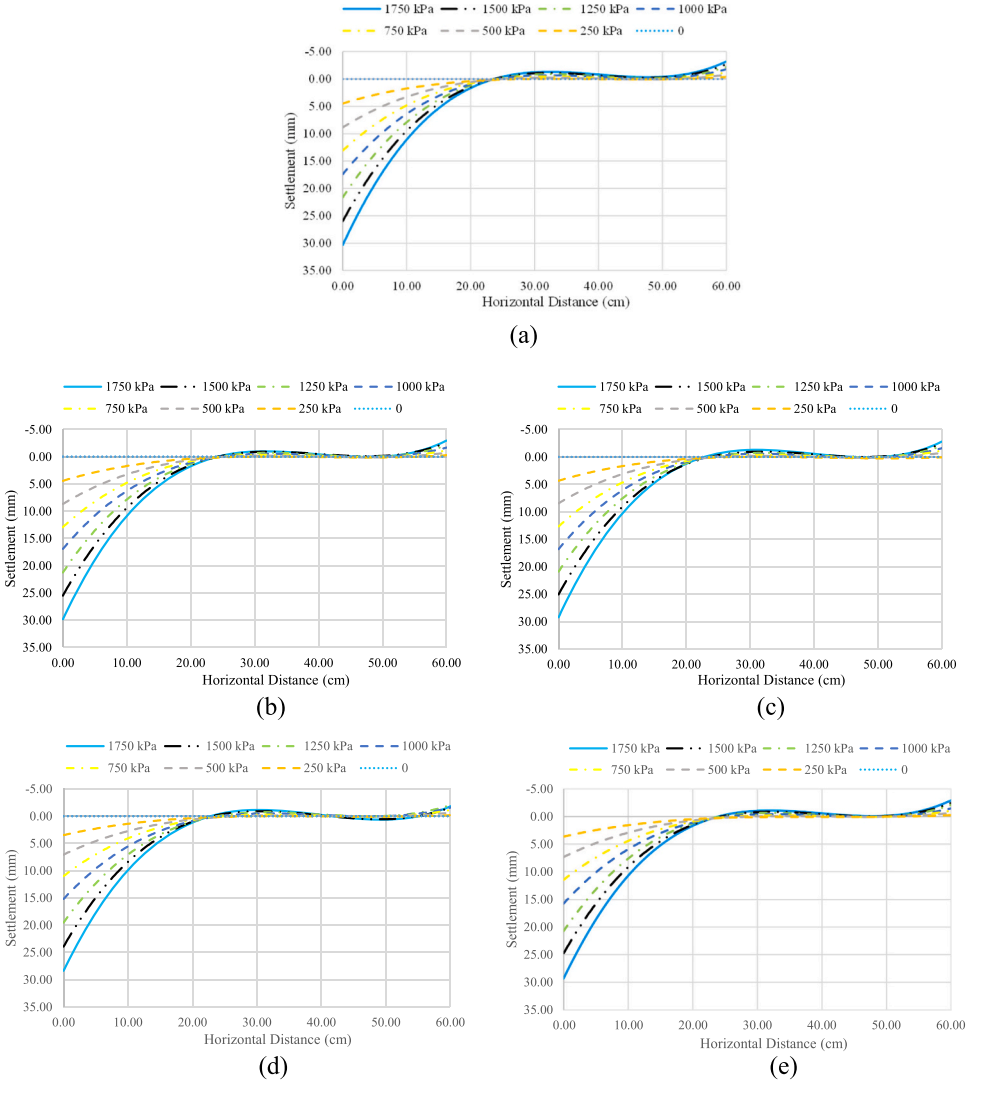

Fig. 9. The change in surface settlements due to applied load level and horizontal distance; (a) Reference section, (b)-(e). Reinforced sections by 440×100, 440×150, 660×100 and 660 × 150 type of geocells, respectively.

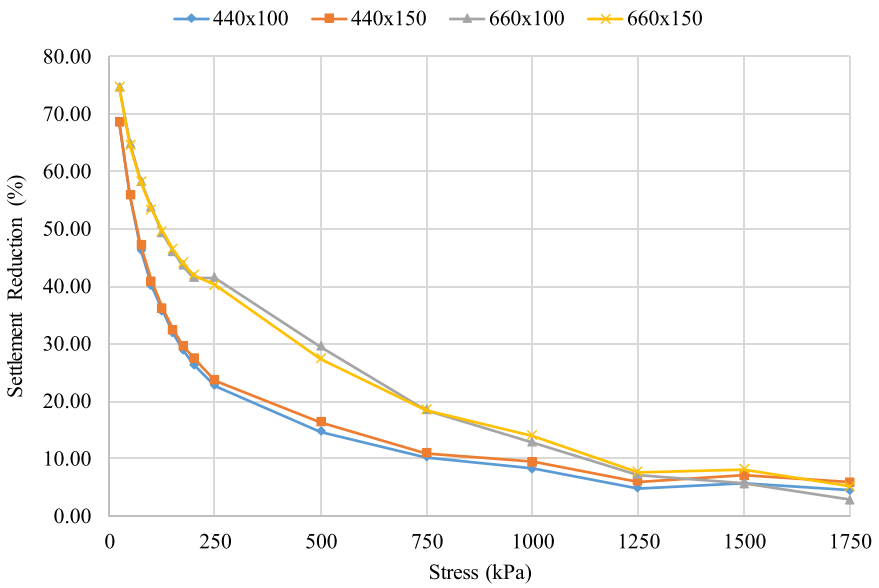

Fig. 10. The change in settlement reduction according to the type of geocell for the finite element model.

addition, this reduction was varied between 77% and 81% with geocell reinforcement usage, even though similar trends were obtained in reinforced sections. The utility of geotextile also affected the stress distribution in the reference section between the two soil layers.

Furthermore, local strain values were collected from strain gauges that fixed on the geocell surfaces without perforation near the center location along vertical direction to validate the settlement behaviour taken from plate load tests. The observed unit deformations in the cell elements increased with the increase of the geocell aperture (Fig. 8(a)). While a strain of 0.012 occurs in a 440×150mm geocell under a vertical stress of 1750 kPa, it reaches a value of 0.016 with a 33% increment in the case of 660×150mm reinforcement usage. However, the 660×100mm type of geocell failed when the stress reached approximately 1600 kPa, and unit strain was observed to be 0.021 due to the large aperture and insufficient cell height (Fig. 8(b)). This result confirms the occurrence of excessive settlement under overload condition including the 660×100mm geocell. It should be noted that the strain data of the section reinforced with 440 × 100 mm geocell are missing on the graph due to an instrument problem. In particular, a general failure mechanism consisting of a serious settlement occurrence in the center location, while heaving behavior becomes dominant at the edges of the box, can be clearly seen in the section improved with the 660×100mm type geocell according to the aforementioned problems.

5.2. Finite element results

When the modeling results were examined in terms of the stress and settlement behaviors considered in the experimental study, the general behavior of settlement values in the center location overlapped (Fig. 5). Numerical results show that the margins of difference between the experimental and numerical analysis in a large-scale box remained below 6.3% for reference section, while the related differences are obtained to be 2.7% under 1750 kPa. The reference settlement was reduced by approximately 25.3% and 36.6% thanks to the 440 and 660 type of geocells, except for the height of the reinforcement. On the other hand, if 50 mm higher geocells are used, they provide the decrease of only 3.4% and 0.3% in the settlement values compared to the 100 mm geocells within same order.

The trend lines of the settlements gradually decreased up to the 40 cm horizontal distance from the center location similar with the experimental ones, while a heaving phenomenon dominated after that, directly (Fig. 9). The modeling results show a slower decrease potential with respect to the increasing distance from the center. It was observed that the change in the settlement data became constant at an average value of 1.3 cm around a 45 cm distance. Due to the load distribution effect of the geocell, the settlements decreased as they moved away from the center and were almost zero at a distance of 45 cm. It was observed that large-aperture geocells spread the load and reduced the settlements more effectively, at these distances. On the other hand, the difference between the experimental data and the modeling analysis at 1000 kPa was determined to be a maximum of 19% in the reinforced section with a 660×100mm geocell, which is noticeable in the numerical analysis in terms of settlement. Contrary to this, the difference is at least 0.5% for a 440 × 150 mm geocell including sections. In addition, the average margin of error in all the experiments was approximately 5.4% under overload conditions, although the difference reached a maximum at 24% for a 660 × 100 mm geocell used under 200 kPa stress. In general, the modeling data were consistent with the experimental results, even though similar behavior was obtained for the geocell reinforced sections. Finite element modeling of the geocell structures may lead to closer results if different approaches are implemented in terms of material details in particular.

The curves regarding the percentage of settlement reduction are given in Fig. 10 with respect to the reference case. According to the results, in the sections reinforced with geocells with 440 mm and 660 mm cell apertures, the settlement values decreased by approximately 27% and 36.8%. Contrariwise, the amount of observed settlement values decreases according to the reduction in

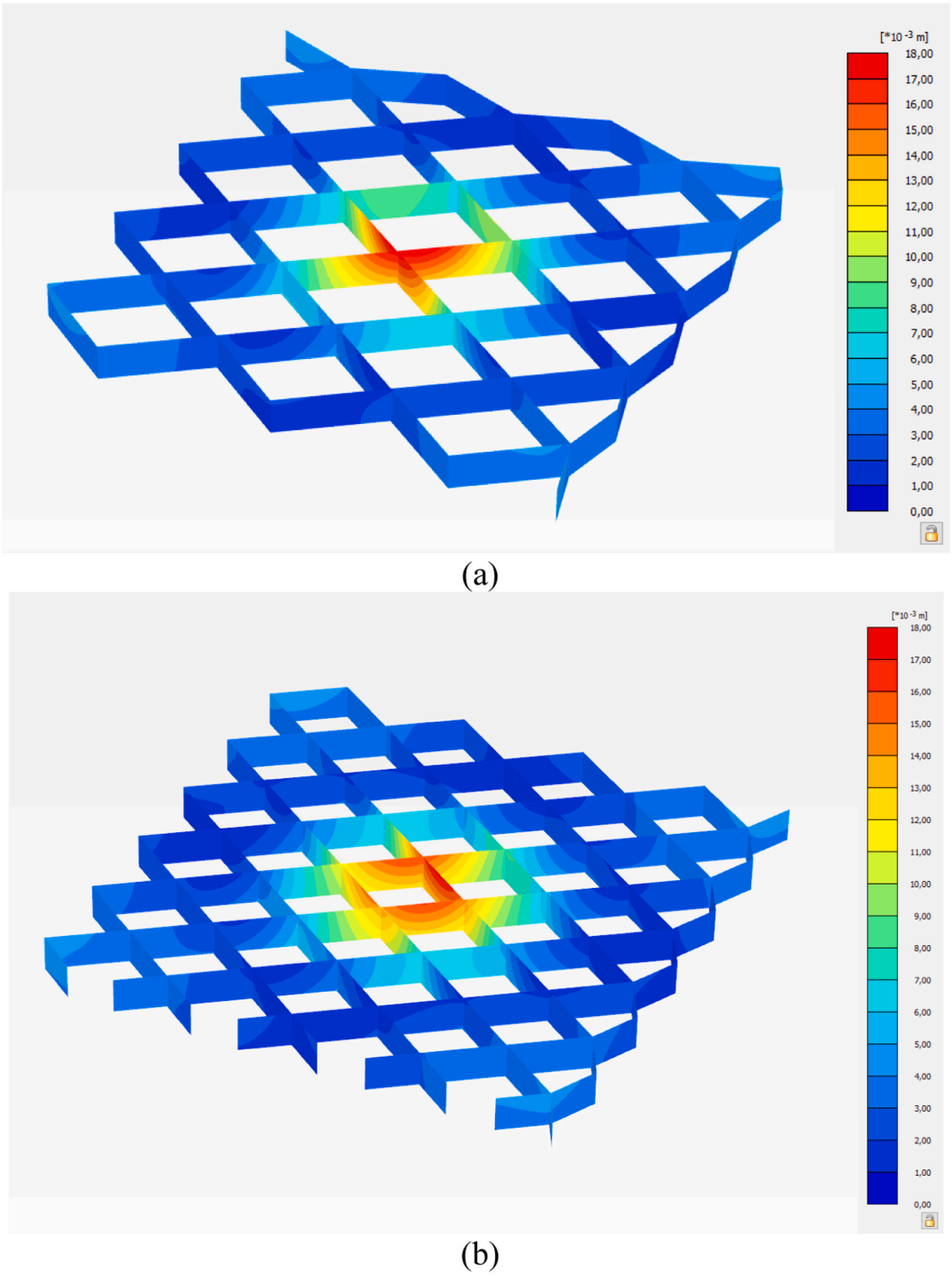

Fig. 11. Deformed shapes of sample geocells with x15 scaling factor after load application, (a) 660 × 100 mm and (b) 440 × 100 mm.

aperture size and the increment in number of the cells per unit area [74–76]. However, the settlement decrease was observed with an increase in the aperture size as mentioned above due to experimental and modeling results in this study. This unexpected behaviour can be explained by the more penetration of the geocell mattress with a high axial stiffness into the subgrade owing to the presence of clay content in the weak layer, before the ultimate confinement effect of 440 mm cell aperture couldn't be attained. This assumption is

proven by the local tearing and failure modes at the midportion of geocell mattresses. Although serious deformations were observed in the experimental geocells with a mesh size of 660 mm, it was observed that the 440 mm geocells preserved their original structure more as well as strain values kept in lower state (Fig. 8). On the other hand, it was determined that if the cell height is 50 mm more, there is a decrease of only 1.8% in the settlement values compared to 100 mm geocells for both aperture values. Therefore, cell aperture is a more effective parameter than cell height. At the end of the modeling process, it is clearly seen that the geocell works within the entire interaction area and the geocells are crushed and shortened, with the nodal points being deformed at the center point where the axial load is at a maximum (Fig. 11). In addition, in all the geocell reinforced sections, the settlement level reached 0 mm and remained constant, where the horizontal location was about 40 cm from the center point.

6. Conclusion

In this study, the effects of geocells types on the settlement potential of two layered road structures are investigated with a large-scale test setup and numerical modeling. In addition to the reference section without geocells, plate loading tests were carried out for 4 different geocell-reinforced sections with cell apertures of 440 mm and 660 mm and cell heights of 100 mm and 150 mm. Based on the gradual loading conditions, the following conclusions may be drawn.

Even though, a sufficient improvement was satisfied between 26% and 59% for 440 mm aperture sized geocells, larger aperture size provided more effective behavior. Similarly, short geocells with a 100 mm cell height enhances the settlement of an unbounded granular layer more effectively at around 10% for low level loading conditions of less than 200kPa. However, this beneficial impact dropped gradually after 200kPa and reached ineffective values at approximately 1000kPa. Interestingly, it even reached values exceeding the reference settlement in case of overloading in 1750 kPa.

Despite the fact that the settlement decreases as the data point moves away from the center location, these values were reset at a distance of approximately 50 cm and 40 cm along the horizontal axis for the experiments and the models, respectively. While the most effective settlement reductions of geocells was obtained around 250 kPa, if the value of 500 kPa was exceeded, it lost its intended use.

The Mohr-Coulomb model results coincided with the experimental results below 5.8% for the reference case, but despite this, a 37.2% difference was detected for the geocell reinforced sections up to 200 kPa stress in particular. If the honeycomb structure of the geocell is drawn closer to reality using splines, unlike equilateral drawing it can be determined in future studies whether the deformations are more consistent moving away from the center.

In general, the loss of confining pressure is leading by the reduction of the stiffness of the geocell-soil composite and the decrease in number of cells per unit area, when the aperture size increased. However, in this study the settlement decrease was observed with an increase in the aperture size. It is thought that the main reason for this situation is that the more penetration behavior of the geocell mattress, which has lower aperture size and higher number of cells per unit area, into the weak subgrade owing to the presence of clay content.

Funding

This research was supported by the Commission of Scientific Research Projects of Eskisehir Technical University (Project Numbers: 21GAP063 and 22ADP096).

CRediT authorship contribution statement

Öztürk Volkan: Data curation, Writing – original draft. **Kara Halil Oğuzhan:** Data curation, Investigation, Visualization, Writing – original draft. **Ucun Muhammed Sefa:** Data curation, Writing – original draft. **Evirgen Burak:** Conceptualization, Methodology, Project administration, Supervision, Writing – review & editing. **Gültekin Asker Alp:** Data curation, Investigation, Visualization, Writing – original draft. **Tos Mert:** Data curation, Investigation, Visualization, Writing – original draft.

Declaration of Competing Interest

The authors declare that they have no known competing financial interests or personal relationships that could have appeared to influence the work reported in this paper.

Data availability

Data will be made available on request.

Acknowledgements

The authors give special thanks to the Istanbul Technical Corporation Research and Development Center for the material support, and to Dr. Emre Akınay for his valuable knowledge during the planning stage.

References

[1] M.A. Khan, A.J. Puppala, Sustainable pavement with geocell reinforced reclaimed-asphalt-pavement (RAP) base layer, J. Clean. Prod. 387 (2023), 135802, https://doi.org/10.1016/j.jclepro.2022.135802.

[2] G. Tavakoli Mehrjardi, S.N. Moghaddas Tafreshi, A.R. Dawson, Combined use of geocell reinforcement and rubber–soil mixtures to improve performance of buried pipes, Geotext. Geomembr. 34 (2012) 116–130, https://doi.org/10.1016/j.geotexmem.2012.05.004.

[3] F.M.P. Aboobacker, S. Saride, M.R. Madhira, Numerical modelling of strip footing on geocell-reinforced beds, Proc. Inst. Civ. Eng.: Ground Improv. 168 (2015) 194–205, https://doi.org/10.1680/grim.13.00015.

[4] A. Hegde, Geocell reinforced foundation beds-past findings, present trends and future prospects: a state-of-the-art review, Constr. Build. Mater. 154 (2017) 658–674, https://doi.org/10.1016/j.conbuildmat.2017.07.230.

[5] V.V. Kumar, S. Saride, Rutting behavior of geocell reinforced base layer overlying weak sand subgrades, Procedia Eng. 143 (2016) 1409–1416, https://doi.org/10.1016/j.proeng.2016.06.166.

[6] N.S. Correia, J.G. Zornberg, Strain distribution along geogrid-reinforced asphalt overlays under traffic loading, Geotext. Geomembr. 46 (2018) 111–120, https://doi.org/10.1016/j.geotexmem.2017.10.002.

[7] S. Saride, S. Gowrisetti, T.G. Sitharam, A.J. Puppala, Numerical simulation of geocell-reinforced sand and clay, Proc. Inst. Civ. Eng.: Ground Improv. 162 (2009) 185–198, https://doi.org/10.1680/grim.2009.162.4.185.

[8] A. Asakereh, M. Ghazavi, S.N. Moghaddas Tafreshi, Cyclic response of footing on geogrid-reinforced sand with void, Soils Found. 53 (2013) 363–374, https://doi.org/10.1016/j.sandf.2013.02.008.

[9] S.N.M. Tafreshi, O. Khalaj, A.R. Dawson, Repeated loading of soil containing granulated rubber and multiple geocell layers, Geotext. Geomembr. 42 (2014) 25–38, https://doi.org/10.1016/j.geotexmem.2013.12.003.

[10] M.I. Onur, M. Tuncan, B. Evirgen, B. Ozdemir, A. Tuncan, Behavior of soil reinforcements in slopes, Procedia Eng. 143 (2016) 483–489, https://doi.org/10.1016/j.proeng.2016.06.061.

[11] J.Q. Wang, L.L. Zhang, J.F. Xue, Y. Tang, Load-settlement response of shallow square footings on geogrid-reinforced sand under cyclic loading, Geotext. Geomembr. 46 (2018) 586–596, https://doi.org/10.1016/j.geotexmem.2018.04.009.

[12] S.M.A.G. Siabil, S.N.M. Tafreshi, A.R. Dawson, Response of pavement foundations incorporating both geocells and expanded polystyrene (EPS) geofoam, Geotext. Geomembr. 48 (2020) 1–23, https://doi.org/10.1016/j.geotexmem.2019.103499.

[13] B. Evirgen, B. Buyuk, G.T. Cil, T. Deger, Experimental performance of polyester-fiber-based soil geogrids against reflective cracks, Transp. Res. Rec. 2675 (2021) 53–64, https://doi.org/10.1177/03611981211027557.

[14] Y. Önal, M. Çalışıcı, C. Kayadelen, G. Altay, A comparative experimental study of geocell and geogrid-reinforced highway base layers under repeated loads, Road. Mater. Pavement Des. 24 (2023) 1–16, https://doi.org/10.1080/14680629.2023.2182126.

[15] N.T. Ngo, B. Indraratna, C. Rujikiatkamjorn, M.M. Biabani, Experimental and discrete element modeling of geocell-stabilized subballast subjected to cyclic loading, J. Geotech. Geoenviron. Eng. 142 (2015), 04015100, https://doi.org/10.1061/(ASCE)GT.1943-5606.0001431.

[16] H. Ahmad, A. Mahboubi, Effect of the interfacial shearing stress of soil–geogrid interaction on the bearing capacity of geogrid-reinforced sand, Innov. Infrastruct. Solut. 6 (2021) 1–13, https://doi.org/10.1007/S41062-020-00430-8.

[17] R. Baadiga, S. Saride, U. Balunaini, M.R. Madhira, Influence of tensile strength of geogrid and subgrade modulus on layer coefficients of granular bases, Transp. Geotech. 29 (2021), 100557, https://doi.org/10.1016/j.trgeo.2021.100557.

[18] J. Chen, X. Guo, R. Sun, S. Rajesh, S. Jiang, J. Xue, Physical and numerical modelling of strip footing on geogrid reinforced transparent sand, Geotext. Geomembr. 49 (2021) 399–412, https://doi.org/10.1016/j.geotexmem.2020.10.011.

[19] E. Cicek, Investigation of effect of geosynthetic reinforcement and placement on road samples with different size, Dicle Univ. J. Eng. 11 (2020) 1307–1317, https://doi.org/10.24012/DUMF.667928.

[20] G. Tavakoli Mehrjardi, R. Behrad, S.N. Moghaddas Tafreshi, Scale effect on the behavior of geocell-reinforced soil, Geotext. Geomembr. 47 (2019) 154–163, https://doi.org/10.1016/j.geotexmem.2018.12.003.

[21] M. Ahmed, M. Abdelhamid, S. Hussain, S. Khedr, T. Breakah, M. Saudy, O. Elkadi, M. Abou-Zeid, Geogrid reinforcement in flexible paved roads, 12th International Transportation Specialty Conference, 104–113, 2019.

[22] A. Shadmand, M. Ghazavi, N. Ganjian, Load-settlement characteristics of large-scale square footing on sand reinforced with opening geocell reinforcement, Geotext. Geomembr. 46 (2018) 319–326, https://doi.org/10.1016/j.geotexmem.2018.01.001.

[23] A. Hegde, T.G. Sitharam, 3-Dimensional numerical modelling of geocell reinforced sand beds, Geotext. Geomembr. 43 (2015) 171–181, https://doi.org/10.1016/j.geotexmem.2014.11.009.

[24] G. Madhavi Latha, A. Somwanshi, Effect of reinforcement form on the bearing capacity of square footings on sand, Geotext. Geomembr. 27 (2009) 409–422, https://doi.org/10.1016/j.geotexmem.2009.03.005.

[25] B. Leshchinsky, H.I. Ling, Numerical modeling of behavior of railway ballasted structure with geocell confinement, Geotext. Geomembr. 36 (2013) 33–43, https://doi.org/10.1016/j.geotexmem.2012.10.006.

[26] H. Venkateswarlu, A. Hegde, Effect of frequency of loading on vibration isolation efficiency of geocell reinforced beds, Sadhana 48 (3) (2023) 129, https://doi.org/10.1007/s12046-023-02198-w.

[27] S. Biswas, M. Hussain, K.L. Singh, Performance evaluation of infill materials of geocell-reinforced granular bed overlying soft subgrade, Indian Geotech. J. 53 (3) (2023) 651–664, https://doi.org/10.1007/s40098-022-00695-z.

[28] M.Y. Abu-Farsakh, J. Gu, G.Z. Voyiadjis, Q. Chen, Mechanistic–empirical analysis of the results of finite element analysis on flexible pavement with geogrid base reinforcement, Int. J. Pavement Eng. 15 (2014) 786–798, https://doi.org/10.1080/10298436.2014.893315.

[29] S.K. Ahirwar, J.N. Mandal, Finite element analysis of flexible pavement with geogrids, Procedia Eng. 189 (2017) 411–416, https://doi.org/10.1016/j.proeng.2017.05.065.

[30] B. Evirgen, M. Tuncan, A. Tuncan, Modelling study on the geotextile, geogrid and steel strip reinforced slopes, Cukurova University, J. Fac. Eng. Archit. 32 (2017) 227–240.

[31] A.C. Nagy, D.V. Moldovan, M. Ciotlaus, L.E. Muntean, Evaluation of experimental and numerical simulation of triaxial geogrid reinforcement on the strength of road structures, Procedia Eng. 181 (2017) 472–479, https://doi.org/10.1016/j.proeng.2017.02.418.

[32] M. Esmaeili, B. Naderi, H.K. Neyestanaki, A. Khodaverdian, Investigating the effect of geogrid on stabilization of high railway embankments, Soils Found. 58 (2018) 319–332, https://doi.org/10.1016/j.sandf.2018.02.005.

[33] W. Li, S. Han, X. Han, Y. Yao, Experimental and numerical analysis of mechanical properties of geocell reinforced reclaimed construction waste composite base layer, Constr. Build. Mater. 304 (2021), 124587, https://doi.org/10.1016/j.conbuildmat.2021.124587.

[34] X. Hong, A numerical study on the application of geocell mat system for buried flexible pipes, KSCE J. Civ. Eng. 27 (4) (2023) 1526–1534, https://doi.org/10.1007/s12205-023-0934-y.

[35] G. Juneja, R.K. Sharma, Numerical study on the behavior of geocell-reinforced sand layer overlying soft clay subgrade, Indian Geotech. J. 53 (2) (2023) 422–436, https://doi.org/10.1007/s40098-022-00689-x.

[36] H. Venkateswarlu, A. Hegde, Behavior of geocell reinforced bed under vibration loading: 3D numerical studies, Geosynth. Int. (2022) 1–20, https://doi.org/10.1680/jgein.21.00050.

[37] S. Sireesh, T.G. Sitharam, S.K. Dash, Bearing capacity of circular footing on geocell–sand mattress overlying claybed with void, Geotext. Geomembr. 27 (2009) 89–98, https://doi.org/10.1016/j.geotexmem.2008.09.005.

[38] S.N.M. Tafreshi, A.R. Dawson, Comparison of bearing capacity of a strip footing on sand with geocell and with planar forms of geotextile reinforcement, Geotext. Geomembr. 28 (2010) 72–82, https://doi.org/10.1016/j.geotexmem.2009.09.003.

[39] S. Davarifard, S.N.M. Tafreshi, Plate load tests of multi-layered geocell reinforced bed considering embedment depth of footing, Procedia Earth Planet. Sci. 15 (2015) 105–110, https://doi.org/10.1016/j.proeps.2015.08.027.
[40] O. Khalaj, S. Davarifard, S.N.M. Tafreshi, B. Mašek, Cyclic response of footing with embedment depth on multi-layered geocell-reinforced bed, World Multidiscip. Earth Sci. Symp. (2016), https://doi.org/10.1088/1755-1315/44/2/022015.
[41] O. Khalaj, S.N.M. Tafreshi, A. Dawson, Pilot-scale load tests of a combined multilayered geocell and rubber-reinforced foundation, Geosynth. Int. 20 (2013) 43–161, https://doi.org/10.1680/gein.13.00008.
[42] ASTM D2487–17. Standard practice for classification of soils for engineering purposes (Unified Soil Classification System). West Conshohocken, 2020.
[43] TS EN ISO 17892–12. Geotechnical investigation and testing - Laboratory testing of soil - Part 12: Determination of liquid and plastic limits - Amendment 2. Ankara, 2022.
[44] TS EN 13286–2. Unbound and hydraulically bound mixtures - Part 2: Test methods for laboratory reference density and water content - Proctor compaction. Ankara, 2013.
[45] TS 1900–2. Methods of testing soils for civil engineering purposes in the laboratory - Part 2: Determination of mechanical properties. Ankara, 2019.
[46] TS EN ISO 17892–3. Geotechnical investigation and testing - Laboratory testing of soil - Part 3: Determination of particle density. Ankara, 2016.
[47] E.M. Palmeira, L.G.S. Antunes, Large scale tests on geosynthetic reinforced unpaved roads subjected to surface maintenance, Geotext. Geomembr. 28 (2010) 547–558, https://doi.org/10.1016/j.geotexmem.2010.03.002.
[48] M. Abu-Farsakh, Q. Chen, R. Sharma, An experimental evaluation of the behavior of footings on geosynthetic-reinforced sand, Soils Found. 53 (2013) 335–348, https://doi.org/10.1016/j.sandf.2013.01.001.
[49] A. Hegde, T.G. Sitharam, Experimental and numerical studies on footings supported on geocell reinforced sand and clay beds, Int. J. Geotech. Eng. 7 (2013) 346–354, https://doi.org/10.1179/1938636213z.00000000043.
[50] M. Kargar, S.M. Mir Mohammad Hosseini, Influence of reinforcement stiffness and strength on load-settlement response of geocell-reinforced sand bases, Eur. J. Environ. Civ. Eng. 22 (2016) 596–613, https://doi.org/10.1080/19648189.2016.1214181.
[51] B. Ok, A. Demir, T. Sarıcı, M. Ovalı, M, Evaluating of geosynthetics reinforced road base with plate loading tests, Pamukkale Univ. J. Eng. Sci. 27 (2021) 718–728, https://doi.org/10.5505/pajes.2016.24483.
[52] TS EN 1849–2. Flexible sheets for waterproofing - Determination of thickness and mass per unit area - Part 2: Plastics and rubber sheets for roof waterproofing. Ankara, 2019.
[53] TS EN ISO 9863–1/A1. Geosynthetics - Determination of thickness at specified pressures - Part 1: Single layers. Ankara, 2020.
[54] TS EN ISO 10319. Geosynthetics - Wide-width tensile test. Ankara, 2015.
[55] TS EN ISO 13426–1. Geotextiles and geotextile-related products - Strength of internal structural junctions - Part 1: Geocells. Ankara, 2020.
[56] TS ISO 18553. Method for the assessment of the degree of pigment or carbon black dispersion in polyolefin pipes, fittings and compounds. Ankara, 2013.
[57] TS EN ISO 1183–1. Plastics - Methods for determining the density of non-cellular plastics - Part 1: Immersion method, liquid pycnometer method and titration method. Ankara, 2019.
[58] R.L. Michalowski, Limit loads on reinforced foundation soils, J. Geotech. Geoenviron. 130 (2004) 381–390, https://doi.org/10.1061/(asce)1090-0241(2004)130:4(381).
[59] M. Chakraborty, J. Kumar, Bearing capacity of circular foundations reinforced with geogrid sheets, Soils Found. 54 (2014) 820–832, https://doi.org/10.1016/j.sandf.2014.06.013.
[60] S. Aria, S.K. Shukla, A. Mohyeddin, Optimum burial depth of geosynthetic reinforcement within sand bed based on numerical investigation, Int. J. Geotech. Eng. 14 (2017) 71–79, https://doi.org/10.1080/19386362.2017.1404202.
[61] TS 1900–1. Methods of testing soils for civil engineering purposes in the laboratory - Part 1: Determination of physical properties. Ankara, 2021.
[62] A. Ari, G. Misir, Three-dimensional numerical analysis of geocell reinforced shell foundations, Geotext. Geomembr. 49 (2021) 963–975, https://doi.org/10.1016/j.geotexmem.2021.01.006.
[63] H.G. Poulos, J.C. Small, Development of design charts for concrete pavements and industrial ground slabs, Thomas Telford, 2000.
[64] E. Panulinova, S. Harabinova, Determination of deformation properties of soils as input parameters for calculation, Matec Web Conferences, 310 (220) 00045. ⟨https://doi.org/10.1051/matecconf/202031000045⟩.
[65] J.E. Bowles, Foundation Analysis and Design, McGraw-Hill, 2001.
[66] B.G. Look, Handbook of Geotechnical Investigation and Design Tables, Taylor & Francis, 2007.
[67] A. Duszynska, A.F. Bolt., Soil - geogrid interaction in pullout test at 2D - deformation conditions, Seventh International Conference on Geosynthetics, 2002.
[68] Bentley, Plaxis 3D-reference manual, 2020.
[69] R.D. Holtz, W.D. Kovacs, T.C. Sheahan, Introduction to Geotechnical Engineering, Pearson, 2010.
[70] B.J. Das, Principles of foundation engineering, Cengage Learning, 2011.
[71] A.B. Göktepe, A. Sezer, Effect of particle shape on density and permeability of sands, Proc. Inst. Civ. Eng.: Geotech. Eng. 163 (2010) 307–320, https://doi.org/10.1680/geng.2010.163.6.307.
[72] A.A. Dinsyah, F. Faris, A. Rifa'i, R.E. Meidudga, Numerical modelling of geocell reinforced slope by use of plastic bottle waste, E3S Web Conf. 325 (2021) 04001, https://doi.org/10.1051/e3sconf/202132504001.
[73] S.K. Pokharel, J. Han, D. Leshchinsky, R.L. Parsons, I. Halahmi, Investigation of factors influencing behavior of single geocell-reinforced bases under static loading, Geotext. Geomembr. 28 (2010) 570–578, https://doi.org/10.1016/j.geotexmem.2010.06.002.
[74] F. Song, H. Liu, B. Yang, J. Zhao, Large-scale triaxial compression tests of geocell-reinforced sand, Geosynth. Int. 26 (2019) 388–395, https://doi.org/10.1680/jgein.19.00019.
[75] F. Song, Y. Jin, H. Liu, J. Liu, Analyzing the deformation and failure of geosynthetic-encased granular soil in the triaxial stress condition, Geotext. Geomembr. 48 (2020) 886–896, https://doi.org/10.1016/j.geotexmem.2020.06.007.
[76] F. Song, W. Chen, Y. Nie, L. Ma, Evaluation of required stiffness and strength of cellular geosynthetics, Geosynth. Int. 29 (2022) 217–228, https://doi.org/10.1680/jgein.21.00032.